03

Electronic, dielectric properties and charge transfer in a $TlGaS_2:Nd^{3+}$ single crystal at direct and alternating current

© S.N. Mustafaeva[1], M.M. Asadov[2,3], S.S. Guseinova[1], A.I. Dzhabarov[1], V.F. Lukichev[4]

[1] Institute of Physics, National Academy of Sciences of Azerbaijan, Baku, Azerbaijan
[2] Nagiev Institute of Catalysis and Inorganic Chemistry of Azerbaijan National Academy of Sciences, Baku, Azerbaijan
[3] Scientific research institute of Geotechnological Problems of Oil, Gas and Chemistry, ASOIU, Baku, Azerbaijan
[4] Valiev Institute of Physics and Technology, Russian Academy of Sciences, Moscow, Russia

E-mail: solmust@gmail.com

Received December 3, 2021
Revised December 3, 2021
Accepted December 8, 2021

The band structure, density of states, and electronic properties of a 32-atomic supercell of a semiconductor compound $TlGaS_2$ containing neodymium are calculated. On the grown new single crystals of $TlGaS_2:Nd^{3+}$ (0.3 mol% Nd_2S_3), experimental results on the physical properties have been obtained. The temperature (93−538 K) and frequency ($5\cdot10^4-3.5\cdot10^7$ Hz) dependences of the dc and ac conductivity and the frequency dispersion of the dielectric coefficients of $TlGaS_2:Nd^{3+}$ single crystals have been studied. It was found that in $TlGaS_2:Nd^{3+}$, in the entire studied frequency range, there are losses due to electrical conductivity, and the charge transfer has a hopping character. The parameters of localized states are estimated, such as the density of localized states near the Fermi level and their spread, the average hopping time and distance, and the concentration of deep traps responsible for the dc and ac conductivity in $TlGaS_2:Nd^{3+}$.

Keywords: DFT calculation, $TlGaS_2$ supercell, neodymium doping, energy structure, density of states, dielectric properties, charge transfer, $TlGaS_2:Nd^{3+}$ single crystal, direct and alternating current.

DOI: 10.21883/PSS.2022.04.53497.251

1. Introduction

The class of thallium chalcogenide compounds of type $TlB^{III}C_2^{VI}$ ($B=$ In, Ga, $C=$ S, Se, Te) is being actively studied for a long time [1]. They have a layered chain structure [2] and anisotropic physical properties. Charge carriers in $TlB^{III}C_2^{VI}$ single crystals can move inside the layers, while their motion between the layers is limited due to van der Waals interaction. Interest to the properties of $TlB^{III}C_2^{VI}$ single crystals is still considerable. Suffice it to say that a biennial international conference on ternary and multicomponent compounds (ICTMC) is held. The properties of the $TlB^{III}C_2^{VI}$ compound, in particular, $TlGaS_2$ are being actively studied [3]. $TlGaS_2$ crystals have both semiconductor and ferroelectric properties. $TlGaS_2$ has the band gap of ~ 2.6 eV at 77 K and is crystallized in a monoclinal unit cell with space group $C2/c$ and parameters: $a=10.299$ Å, $b=10.284$ Å, $c=15.175$ Å, $\beta=99.603^\circ$ [1,2].

Electric, photoelectric, X-ray dosimetry properties of $TlGaS_2$ single crystals and influence of lithium ion intercalation on them have been studied [1]. The influence of impurities, e.g., transition metals (Fe, Co, Ni) [4–6] and heavy lanthanoids (Er, Yb) [3,5] on electric and dielectric properties of $TlGaS_2$ single crystals has been also studies. The main attention in the corresponding studied was paid to stability of some or other properties of the $TlGaS_2$ single crystal. However, so far there is no systematic data on physical properties of lanthanoid-doped $TlGaS_2$ single crystals.

Lanthanoid sesquisulfides (Ln_2S_3, where Ln=La−Lu) attract researchers-attention thanks to their interesting structural, optical, magnetic and thermoelectric properties [7]. In such wide-band-gap semiconductor sulfides of trivalent lanthanoids, $4f$-electrons are localized in the inner shell of lanthanoid ions, while polarization of $5d$-electrons leads to ferro- and antiferromagnetic interactions in lanthanide alloys [8].

Ln_2S_3 compounds exist in the form of several polymorphic modifications: $\alpha, \beta, \gamma, \delta$ and ε. The α-phase has an orthorhombic structure and is a low-temperature phase. The β-phase has a tetragonal structure and a variable composition $Ln_{10}S_{14}O_{1-x}S_x$ $(0\le x\le 1)$. The γ-phase has a cubic defect structure of the Th_3P_4 type and is a high-temperature phase of Ln_2S_3. The δ-phase has a monoclinic structure, while the ε-phase has a rhombohedral structure [9]. In particular, the Nd_2S_3 compound has two polymorphic modifications [9–11]: α (space group $Pnma$) and γ-phases (space group $I\bar{4}3d$). Paper [12] showed that the absorption, excitation and luminescence spectra contain bands related to $4f-4f$-transitions of trivalent ions Pr^{3+} and Nd^{3+} in double molybdates.

An analysis of the experimental results for doped $TlGaS_2$ single crystals [1–6] shows that the monoclinic (space group

$C2/c$) structure retains the same symmetry as a result of an ordered distribution of doping atoms in interstices and in the sublattice of Ga atoms. Taking this into account, the obtaining of single crystals of new compositions $TlGaS_2$, activated by trivalent neodymium ions (Nd^{3+}) can be used to create functional materials.

Single crystals of neodymium-containing ternary chalcogenides are poorly studied. Various phase transformations occur in semiconductor materials containing Ln^{3+}. There are exchange interactions of Ln^{3+} ions and chalcogenide metals whose valence electrons with the highest energy occupy the *p*-orbital. For instance, selenides Ln^{3+} are characterized by interaction and hybridization between localized $4f$- and meandering $5d$-electrons [6]. Therefore, partial substitution of gallium by neodymium (Nd) can considerably affect the physical properties of $TlGaS_2$. However, the regularities of frequency dispersion of dielectric coefficients and charge transfer in neodymium-containing $TlGaS_2$ have not been studied. In the present paper, we analyzed the band structure for the monoclinic (sp. gr. $C2/c$) phase on the basis of $TlGaS_2:Nd^{3+}$, determined the structural parameters and calculated the density of atoms' (ions) state in the $TlGaS_2$ structure. We compared three $TlGaS_2$-based band structures to determine its electronic properties. In addition to the aforesaid, the present paper was aimed at determining the dielectric parameters of the $TlGaS_2$ single crystal, containing a dopant of Nd^{3+} ions (0.3 mol.% Nd_2S_3) and at establishing the mechanism of direct current conductivity (dc-conductivity — σ_{dc}) and alternating current conductivity (ac-conductivity — σ_{ac}).

2. Experimental and calculation procedure

2.1. Synthesis

The initial chemical substances used in this study to obtain single-crystal samples of $TlGaS_2:Nd^{3+}$ were the $TlGaS_2$ compound and the low-temperature modification of dineodymium trisulfide α-Nd_2S_3.

$TlGaS_2$ was synthesized using Tl (Tl00), Ga (Ga $5N$), S (extra-pure 165). $TlGaS_2$ was synthesized in an electric furnace by interaction of stoichiometric amounts of thallium, gallium and sulfur at 1000 ± 5 K for 5–7 h in a quartz ampule sealed under vacuum 10^{-3} Pa [3,13]. Temperature of the furnace, containing the ampule with the Tl, Ga and S components, was increased from 870 to 1000 K for 2 h, to avoid an explosion due to the high sulfur vapor pressure.

The low-temperature modification of α-Nd_2S_3 was synthesized from neodymium oxide powders (Nd_2O_3) as per the procedure described in [14–16]. The reaction of Nd_2O_3 sulfurization in a tube furnace was carried out using CS_2 gas at 1123 K for 3 h. Synthesis completion, homogeneity, individuality of $TlGaS_2$ and α-Nd_2S_3 was monitored by the XRF method (D8 Advance Bruker AXS diffractometer; CuK_α-radiation) in the angle range of 2θ: 10–100°.

The samples of $TlGaS_2:Nd^{3+}$ (0.3 mol.% Nd_2S_3) were obtained by melting together of stoichiometric weighed portions of previously prepared initial components $TlGaS_2$ and α-Nd_2S_3 in quartz ampules evacuated to 10^{-3} Pa and sealed. Single crystals were grown from the synthesized samples of $TlGaS_2:Nd^{3+}$ by the Bridgman–Stockbarger method. To do so, the synthesized $TlGaS_2:Nd^{3+}$ polycrystals were ground and in the ground state placed in a quartz ampule 8–10 cm long, with the internal diameter of 1 cm and a pointed end. The quartz ampule with the sample of $TlGaS_2:Nd^{3+}$, evacuated to a residual pressure not worse than 10^{-3} Pa, was placed in a dual-temperature electric furnace of the unit for single crystal growing. The temperature of 1165 ± 10 K was maintained in the furnace top, and 1110 ± 10 K — in the bottom. The speed of ampule movement in the furnace was equal to 0.3–0.5 cm/h, while temperature gradient at the crystallization front was 25 ± 5 K.

The surface of the obtained $TlGaS_2:Nd^{3+}$ single crystal was mirror-smooth, and the single crystal was used for physical studied without additional treatment.

2.2. Electric measurements

The samples of $TlGaS_2:Nd^{3+}$ for direct- and alternating current electric measurements were made in a sandwich variant, i.e. the external electric field was applied across the natural crystal layers (along the crystal *C*-axis). Silver paste was used as electrodes to the samples. Intensity of the electric field applied to the crystals corresponded to the ohmic region of the current-voltage characteristic. Direct-current conductivity of the samples was measured using the PIUS-1UM-K instrument, the temperature range of electric measurements being 93–538 K. The sample temperature was measured using a remote temperature sensor with the error of ± 0.2 K. Dielectric coefficients of the $TlGaS_2:Nd^{3+}$ crystals were measured by the resonance method [17] using a Q-meter. The range of alternating electric field frequencies was $5 \cdot 10^4 - 3.5 \cdot 10^7$ Hz. All dielectric measurements were performed at 300 K. Reproducibility of the resonance position was ± 0.2 pF in terms of capacitance, and $\pm 1.0 - 1.5$ scale division in terms of quality factor ($Q = 1/\mathrm{tn}\delta$). Thereat, the largest deviations from the average values were 3–4% for ε and 7% for tnδ.

2.3. Calculation procedure

The band structure and electron states of $TlGaS_2$ and $TlGaS_2:Nd^{3+}$ semiconductor crystals were studied within the framework of the density functional theory (DFT). The Atomostix ToolKit software package was used. The interatomic distance for theoretical calculations was calculated within the framework of Generalized Gradient Approximation (GGA) and local density approximation (LDA and LSDA). Integration within the reduced Brillouin zone was performed using *k*-points $2 \times 2 \times 2$ according to the Monkhorst–Pack scheme. The electronic structure of $TlGaS_2$ and $TlGaS_2:Nd^{3+}$ was calculated for equilibrium

lattice parameters [18,19]. The latter were obtained by minimizing the total energy for each calculation scheme. The crystalline structure was optimized until the maximum value of the interatomic force was less than 0.01 eV/Å, while the maximum value of the mechanical stress tensor was less than 0.01 eV/A^3. The hybrid method was used to increase accuracy of band gap underestimation [20]. The exchange and correlation potentials for DFT-calculations were corrected using the Hubbard model [21].

3. Results and discussion

Fig. 1 shows the X-ray diffraction patterns for the initial compounds $TlGaS_2$ and Nd_2S_3. The X-ray images have distinct reflections corresponding to the $TlGaS_2$ and Nd_2S_3 crystals. They are identified by a monoclinic structure with a space group (sp. gr.) $C2/c$ for $TlGaS_2$ and an orthorhombic modification (sp. gr. $Pnma$) Nd_2S_3. The structural characteristics of the $TlGaS_2$ compound ($a = 10.299$ Å, $b = 10.284$ Å, $c = 15.175$ Å, $\beta = 99.603°$) agree with the data of [1,2,22,23]. The X-ray image for the synthesized Nd_2S_3 corresponded to the following structural data for the orthorhombic α-phase of α-Nd_2S_3: $a = 4.028 \pm 0.001$, $b = 7.447 \pm 0.001$, $c = 15.519 \pm 0.002$ Å. These parameters agree with the structural data of α-Nd_2S_3 in [9,24].

3.1. DFT-studies

The initial model will be the results of the DFT-study of a 32 atom supercell of $TlGaS_2$ (Fig. 2). Atoms of the first and second layers for correct reproduction of the electronic structure of the bulk were fixed in equilibrium „perfect" positions of the bulk lattice, atoms of the other „upper" layers were able to relax.

Fig. 2 shows the optimized atomic model of $TlGaS_2$ (Fig. 2, *a*), where one Ga atom at the specified positions was successively substituted by a Nd atom (Fig. 2, *b*). The calculated values of total energy of the obtained structures and their difference from the minimum possible energy have shown that the energy increment did not exceed 0.13 eV. Substitution of one Ga atom with a Nd atom in the $TlGaS_2$ supercell does not greatly change the total energy (the maximum change is 0.1 eV). Moreover, if we increase the layers in the model, placement of Nd atoms in the surface layer is preferable, as compared to placement in the middle layer.

Substitution of a gallium atom with a neodymium atom in the $TlGaS_2$ supercell causes a change of distance ($\leftrightarrow$) between the layers. Thus, the distance between the second and third layers in neodymium-containing structures is larger than the bulk distance, while in pure $TlGaS_2$ it is smaller. Addition of a neodymium atom leads to a successive increase of the distance between the model layers. In particular, when the 12-th Ga atom in the $TlGaS_2$ supercell is substituted by a Nd atom, the calculated distances between S atoms around Nd significantly differ from each other. For instance, distances between the 12-th Nd atom and the 21-st one (for $Nd_{12} \leftrightarrow S_{21} - 2.017$ Å), 25-th (for $Nd_{12} \leftrightarrow S_{25} - 2.295$ Å) and 29-th S atoms (for $Nd_{12} \leftrightarrow S_{29} - 2.534$ Å) differ from each other.

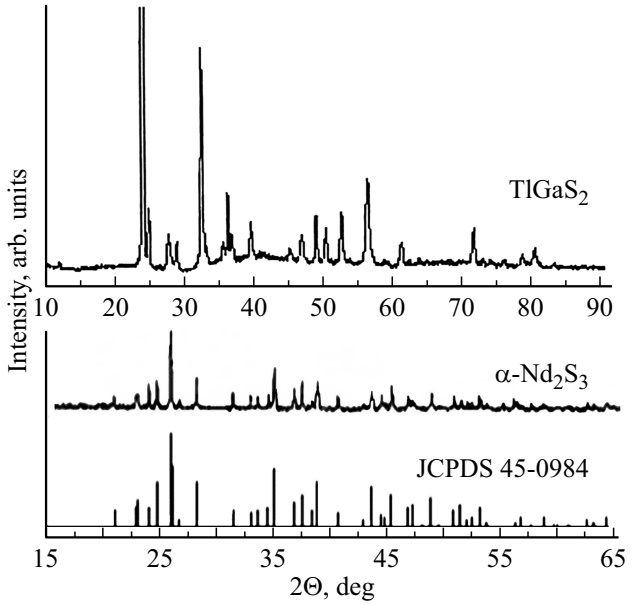

Figure 1. X-ray diffraction patterns for the initial compounds $TlGaS_2$ and α-Nd_2S_3.

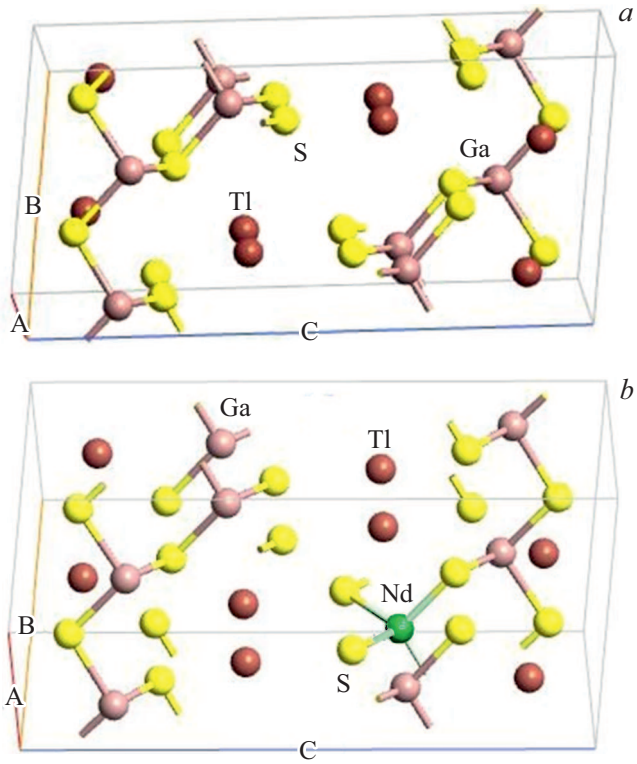

Figure 2. Atomic model of the studied $TlGaS_2$ and $TlGaS_2:Nd^{3+}$ supercells: *a* — primitive cell of the $TlGaS_2$ compound; *b* — $TlGaS_2:Nd^{3+}$ supercell where one Ga atom is substituted by a Nd atom.

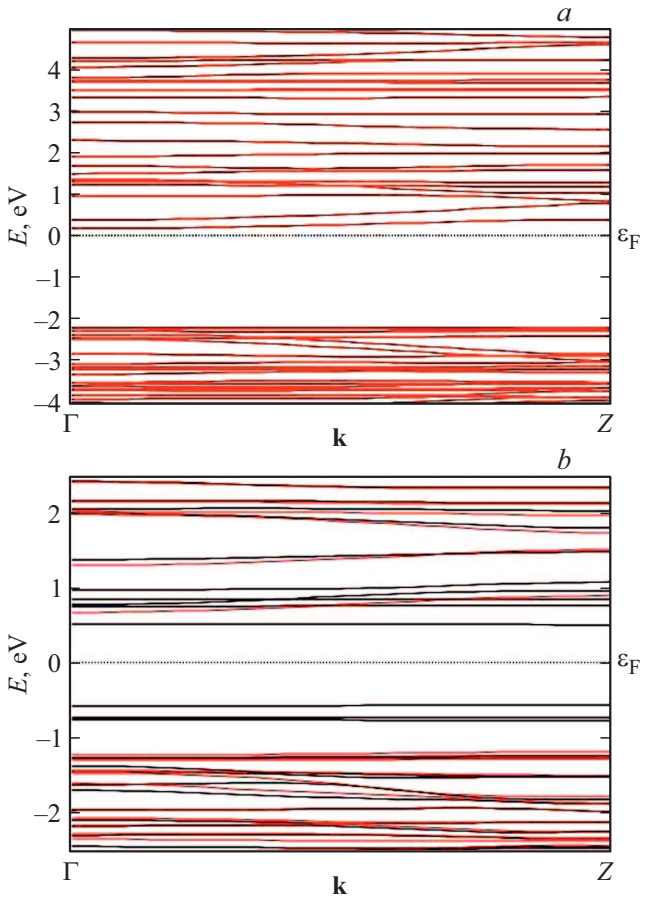

Figure 3. Band structure of $TlGaS_2$ (a) and $TlGaS_2:Nd^{3+}$ crystals (b) (the LSDA calculation scheme taking into account the Hubbard model was used). The states in the negative energy region pertain to the valence band, and in the positive energy region — to the conduction band.

The band structures and densities of states(DOS), constructed with the framework of the used approximation, for the $TlGaS_2$ and $TlGaS_2:Nd^{3+}$ crystals are qualitatively equal. We solved the problem of mismatch between the DFT-calculated value of the band gap with the experimental data of E_g by using a Hubbard model [21] that describes particle interaction in a lattice

$$H = \sum_{i,j}\sum_{\sigma} T_{ij} c^{+}_{i\sigma} c^{-}_{j\sigma} + \frac{1}{2} I \sum_{\sigma,i} U_i n_{i,\sigma} n_{i,-\sigma} - I \sum_{\sigma,i} v_{ii} n_{i\sigma}, \tag{1}$$

where T_{ij} — transfer integral that describes electron hopping from site i to site j; $c^{+}_{i\sigma}$ and $c^{-}_{j\sigma}$ — operators of birth and elimination of electrons with spin σ at site i; $c^{+}_{i\sigma} c^{-}_{j\sigma} = n_{i\sigma}$ — operator of the number of particles with spin σ at site i; U_i — Coulomb repulsion energy of two electrons being at the i-th site; integral $I = (ii|1/r|ii)$; $v_{ii} = \frac{1}{2} n$.

This model makes it possible to approximate electron states in narrow energy bands, in particular, the energy of single-electron atomic state at site i. The Hamiltonian of this model contains, in addition to the intrinsic energy of electrons, a kinetic term that corresponds to particle tunneling between lattice sites, and a term that describes Coulomb repulsion of two electrons being at one lattice site.

Fig. 3 shows the band structure only for the hybrid LSDA scheme that comprises correction parameters. On the whole, the obtained results agree satisfactorily with the experimental data of $E_g = 2.62$ eV at 77 K [2]. The obtained models of the crystal band structure show a decreased value of the band gap to 2.39 eV (for pure $TlGaS_2$) as compared to the experimental E_g (Fig. 3, a). A similar decrease of E_g was also observed for $TlGaS_2:Nd^{3+}$ (Fig. 3, b).

It was established that the value of E_g decreases as a result of neodymium doping of $TlGaS_2$. This can be associated with compensation of electrically active impurity centers in the $TlGaS_2$ monoclinic structure by interstitial energy levels of neodymium ions. The arising structural defects due to $TlGaS_2$ crystal doping stimulate the migration of defects present in the crystal.

Densities of states for the valence band and subbands of the $TlGaS_2:Nd^{3+}$ structure are shown in Fig. 4. Substitution of one gallium atom with a neodymium atom in $TlGaS_2$ causes a redistribution of electrons of the s-, p- and d-shells of the neodymium atom and formation of hybridized $TlGaS_2:Nd^3$ states. A successive increase of the quantity of Nd atoms reduces the density of states for relative energies in $TlGaS_2:Nd^3$. A transition from the s-state of the Nd atom to the p- and d-states in $TlGaS_2:Nd^3$ reduces the density of states for relative energies, both for the „spin up“configuration and for the „spin down“ configuration (Fig. 4, a, b, c).

3.2. Direct current conductivity of $TlGaS_2:Nd^{3+}$ (dc-conductivity)

Fig. 5 shows the high-temperature dependence of the ohmic direct-current conductivity of $TlGaS_2:Nd^{3+}$ in $\lg\sigma_{dc}$ coordinates on $10^3/T$. An exponential area with a slope of 0.1 eV was observed on the dependence of $\lg\sigma_{dc}$ on $10^3/T$ in the temperature region of 303−538 K. When temperature decreased, conductivity activation energy did not have a constant slope.

The low-temperature dependence of conductivity of $TlGaS_2:Nd^{3+}$ was re-plotted in Mott coordinates $\lg\sigma_{dc}$ vs. $T^{-1/4}$ in the temperature range of 93−188 K and is shown in Fig. 6. As seen from Fig. 6, all the experimental points fitted well in these coordinates on the straight line. This dependence $\lg\sigma_{dc}$ on $T^{-1/4}$ indicates than conduction is performed by charge carrier hops on states lying near the Fermi level [25]

$$\sigma \sim \exp\lfloor -(T_0/T)^{1/4} \rfloor, \tag{2}$$

$$T_0 = \frac{16}{N_F k_B a^3}, \tag{3}$$

where k_B — Boltzmann constant, a — localization radius, N_F — density of localized states near the Fermi level.

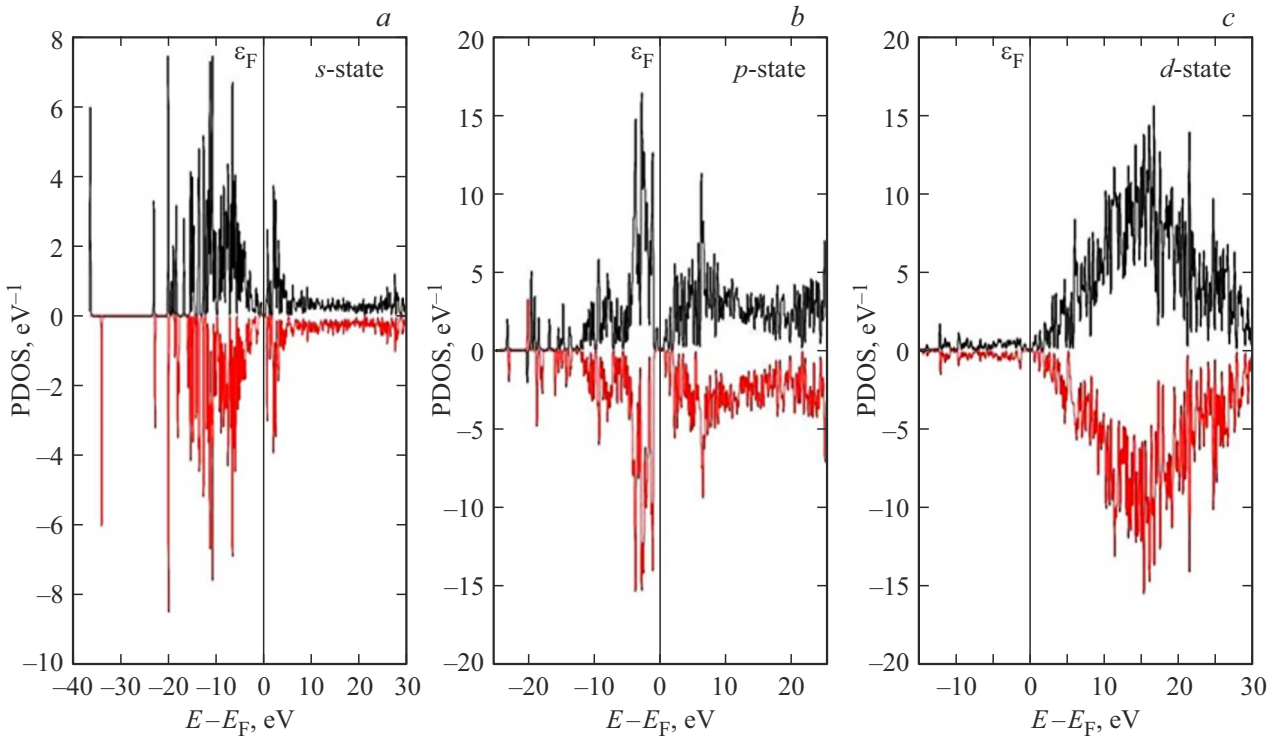

Figure 4. Local partial densities of states (PDOS) for the *s*-, *p*- and *d*-shells of neodymium (*a, b, c*, respectively) in the $TlGaS_2:Nd^{3+}$ compound with a tetrahedral coordination of Nd atom. The dashed line shows the Fermi level; the black line — the spin „up" state; the red line — the spin „down" state.

From the slope of the low-temperature dependence of $\lg\sigma_{dc}$ on $T^{-1/4}$ we have determined the value of T_0, which was equal to $T_0 = 1.7 \cdot 10^6$ K, and we have used formula (3) to estimate the density of states in $TlGaS_2:Nd^{3+}$: $N_F = 4 \cdot 10^{19}\,eV^{-1} \cdot cm^{-3}$. The value $a = 14$ Å was taken for the localization radius similarly to $TlGaS_2$ [17] when estimating N_F.

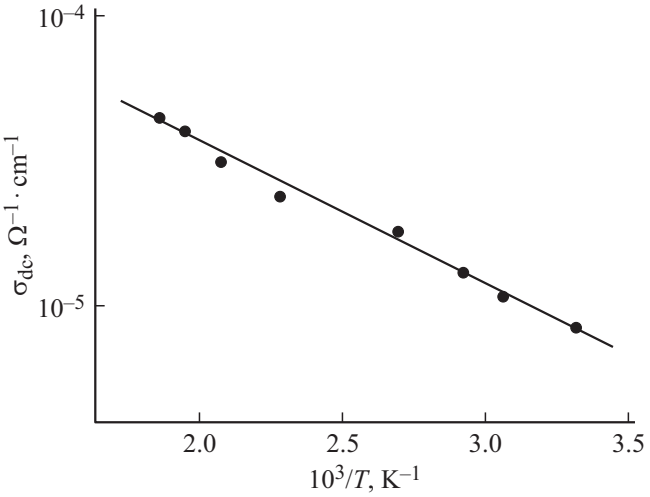

Figure 5. High-temperature dependence of conductivity of $TlGaS_2:Nd^{3+}$ (0.3 mol.% Nd_2S_3) in the temperature range of 303–538 K in Arrhenius coordinates.

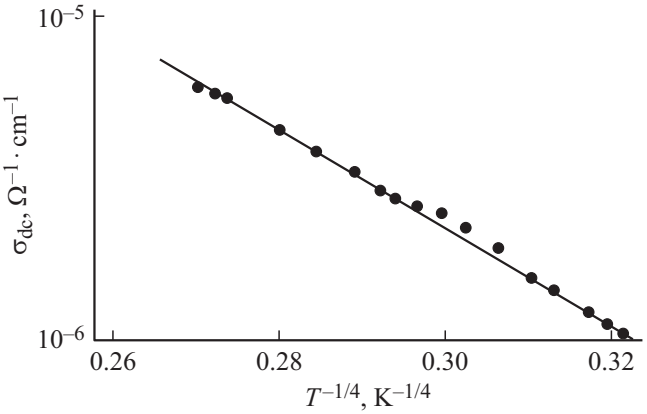

Figure 6. Low-temperature conductivity of $TlGaS_2:Nd^{3+}$ (0.3 mol.% Nd_2S_3) in the temperature range of 93–188 K in Mott coordinates.

We have also estimated the hop distances R of charge carriers in $TlGaS_2:Nd^{3+}$ at different temperatures

$$R = \frac{3}{8}\, a\, T_0^{1/4} T^{-1/4}. \qquad (4)$$

For instance, at $T = 93$ K $R = 61$ Å, while at $T = 188$ K $R = 51$ Å, so that the average hop distance in $TlGaS_2:Nd^{3+}$ in the temperature region of 93–188 K was $R_{av} = 56$ Å. The value of R_{av} was 4 times larger than the average

distance between the charge carrier localization centers, i.e. $R_{av}/a = 4$.

From the condition [25]:

$$\frac{4\pi}{3} R^3 \cdot N_F \cdot \frac{\Delta E}{2} = 1 \quad (5)$$

we estimated the spread of trap states near the Fermi level: $\Delta E = 68$ meV. The concentration of deep traps in $TlGaS_2:Nd^{3+}$, estimated using the formula $N_t = N_F \Delta E$, was $N_t = 2.7 \cdot 10^{18}$ cm^{-3}.

Temperature dependence of activation energy in the region of hopping conductivity with a variable hop length is described by the relation [26]:

$$\Delta W = \frac{(k_B T)^{3/4}}{(N_F \cdot a^3)^{1/4}}. \quad (6)$$

The average hop activation energy in $TlGaS_2:Nd^{3+}$ according to formula (6) was 62 meV in the temperature range of 93–188 K.

Thus, hopping conductivity with a variable length of hop on states, localized near the Fermi level, takes place in $TlGaS_2:Nd^{3+}$ in the temperature region of 93–188 K.

3.3. Alternating current conductivity of $TlGaS_2:Nd^{3+}$ (ac-conductivity)

Hopping conductivity in $TlGaS_2:Nd^{3+}$ in alternating electric fields was also studied. Fig. 7 shows the frequency dependence of ac-conductivity of $TlGaS_2:Nd^{3+}$ in the range of $f = 5 \cdot 10^4 - 3.5 \cdot 10^7$ Hz at $T = 300$. It should be noted that, as compared to $TlGaS_2$ [3], conductivity of $TlGaS_2:Nd^{3+}$ are approximately by an order higher in the entire frequency range from $5 \cdot 10^4$ to $3.5 \cdot 10^7$ Hz. Fig. 7 shows that σ_{ac} conductivity for $TlGaS_2:Nd^{3+}$ up to the frequency $f = 2 \cdot 10^5$ Hz little depends on frequency, while conductivity vs. frequency at higher frequencies up to $3.5 \cdot 10^7$ Hz is described by a power law $\sigma_{ac} \sim f^n$, where $n = 0.8$.

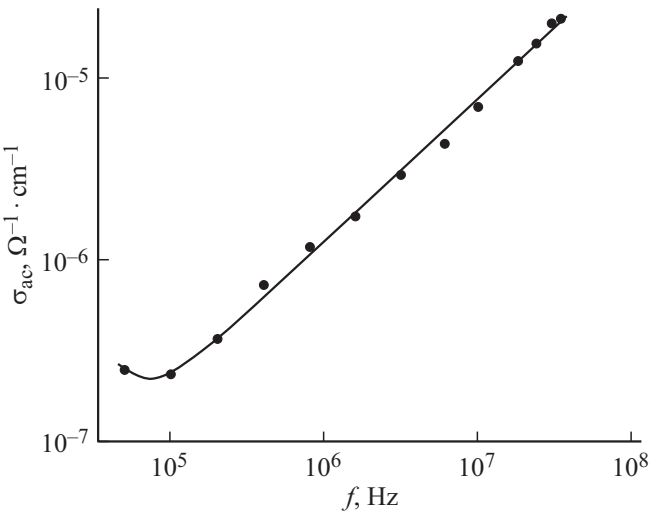

Figure 7. Frequency-dependent conductivity of $TlGaS_2:Nd^{3+}$ (0.3 mol.% Nd_2S_3) at $T = 300$ K.

Ac-conductivity of the band type in semiconductors is known [25] to be chiefly frequency-independent up to $10^{10}-10^{11}$ Hz. The observed experimental dependence $\sigma_{ac} \sim f^{0.8}$ in $TlGaS_2:Nd^{3+}$ indicates that it is due to charge carrier hops between the states localized in the band gap. These can be states localized near the allowed band edges or states localized located near the Fermi level in the $TlGaS_2:Nd^{3+}$ crystal. In the experimental conditions, conductivity on states near the Fermi level always prevails over conductivity on states near the allowed band edges. The obtained law $\sigma_{ac} \sim f^{0.8}$ in $TlGaS_2:Nd^{3+}$ crystals means a hopping mechanism of charge transfer on states localized in the Fermi level vicinity.

According to [27]:

$$\sigma_{ac}(f) = \frac{\pi^3}{96} e^2 k_B T N_F^2 a^5 f \left[\ln\left(\frac{\nu_{ph}}{f}\right)\right]^4, \quad (7)$$

where e — electron charge; $a = 1/\alpha$ — localization radius; α — constant of decrease of the wave function for a localized charge carrier $\psi \sim e^{-\alpha r}$; ν_{ph} — phonon frequency.

According to formula (7), ac-conductivity depends on frequency as $f[\ln(\nu_{ph}/f)]^4$, i.e. at $f \ll \nu_{ph}$ the quantity σ_{ac} is proportional to $f^{0.8}$.

We used formula (7) calculate the density of states at the Fermi level according to the experimentally determined values of $\sigma_{ac}(f)$. The calculated value of N_F for $TlGaS_2:Nd^{3+}$ was $N_F = 2.2 \cdot 10^{19}$ eV$^{-1} \cdot$ cm^{-3}. As has been shown above, the value of N_F obtained by direct current measurements was $N_F = 4 \cdot 10^{19}$ eV$^{-1} \cdot$ cm^{-3}. The value of N_F in $TlGaS_2$ was by almost an order smaller, $5.9 \cdot 10^{18}$ eV$^{-1} \cdot$ cm^{-3} [3]:

According to the alternating current hopping conductivity, the average hop distance (R) is determined using the following formula

$$R = \frac{1}{2\alpha} \ln\left(\frac{\nu_{ph}}{f}\right). \quad (8)$$

The value of R calculated using formula (8) for $TlGaS_2:Nd^{3+}$ was 77 Å. The value of R made it possible to use the formula

$$\tau^{-1} = \nu_{ph} \cdot \exp(-2\alpha R) \quad (9)$$

to determine the average hop time in $TlGaS_2:Nd^{3+}$: $\tau = 5.7 \cdot 10^{-8}$ s.

3.4. Dielectric properties

We also studied the frequency dependence of dielectric coefficients for $TlGaS_2:Nd^{3+}$: complex permittivity and tangent of dielectric loss angle ($\mathrm{tn}\delta$). Fig. 8, *a, b* and Fig. 9 show the experimentally obtained frequency dependences of the real (ε') and imaginary (ε'') parts of complex permittivity and $\mathrm{tn}\delta$ in $TlGaS_2:Nd^{3+}$ at 300 K. The dependence

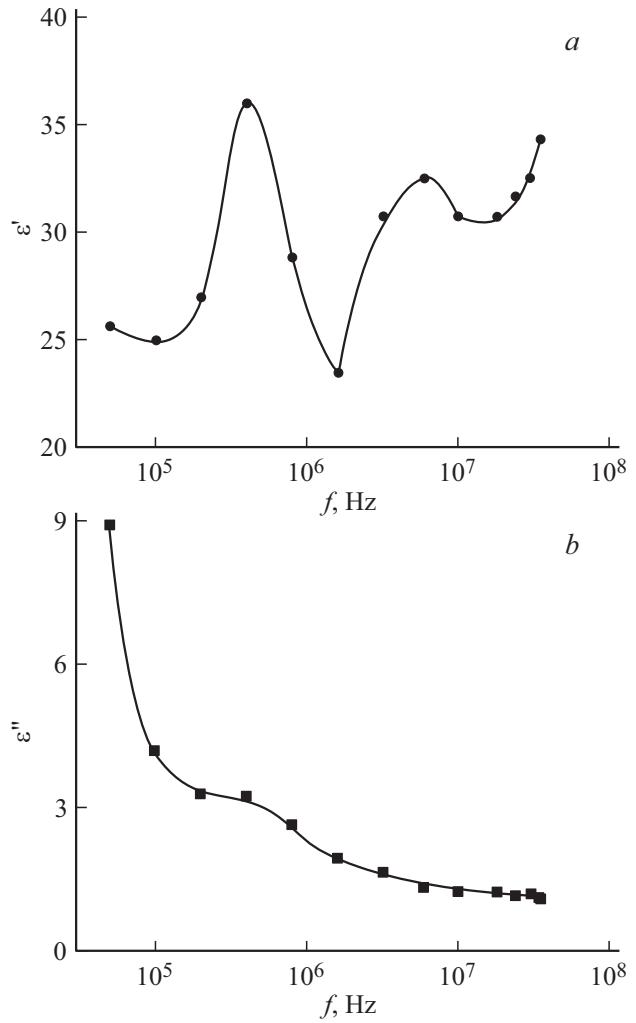

Figure 8. Frequency dispersion of the real (a) and imaginary (b) parts of complex permittivity of the $TlGaS_2:Nd^{3+}$ crystal (0.3 mol.% Nd_2S_3). $T = 300$ K.

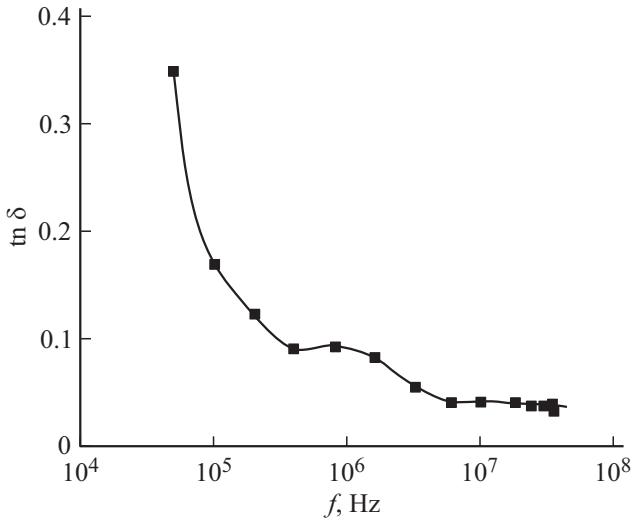

Figure 9. Frequency dependence of the tangent of dielectric loss angle in $TlGaS_2:Nd^{3+}$ (0.3 mol.% Nd_2S_3) at $T = 300$ K.

tn$\delta(f)$ had a hyperbolic decrease of the tangent of dielectric loss angle with frequency increase (Fig. 9). This indicates losses due to electrical conductivity [28] in $TlGaS_2:Nd^{3+}$.

4. Conclusion

It has been established that the grown $TlGaS_2:Nd^{3+}$ single crystals (0.3 mol.% Nd_2S_3) (a monoclinic structure with space group $C2/c$; $a = 10.299$ Å, $b = 10.284$ Å, $c = 15.175$ Å, $\beta = 99.603°$) have a high resistivity and band gap $E_g = 2.45$ eV at 300 K. The DFT-calculations of the band and electronic structure in the supercell of the $TlGaS_2$ semiconductor compound with 32 atoms made it possible to determine the kind of electron density and agree the calculated values $E_g = 2.39$ (taking into account the Hubbard model in a static fluctuation approximation) and the experimental values of E_g. A comparison of the band structure of $TlGaS_2$ and $TlGaS_2:Nd^{3+}$ single crystals indicates that the value of compound's E_g decreases due to neodymium doping of $TlGaS_2$. A decrease of the band gap of doped $TlGaS_2:Nd^{3+}$ can be associated with the compensation of the initial electrically active impurity centers by energy levels of neodymium ions. Doping of the $TlGaS_2:Nd^{3+}$ single crystal gives rise to structural defects and stimulates the migration of defects existing in the crystal.

The measurements of the physical properties of the $TlGaS_2:Nd^{3+}$ single crystal (0.3 mol.% Nd_2S_3) at 93–538 K and frequencies $5 \cdot 10^4 - 3.5 \cdot 10^7$ Hz made it possible to determine the dielectric characteristics and their frequency dispersion. It has been found that dielectric losses are associated with losses of reach-through conductivity in $TlGaS_2:Nd^{3+}$. It has been found that, direct-current and alternating-current hopping conductivity on states, localized near the Fermi level, occurs in $TlGaS_2:Nd^{3+}$. We have determined density ($N_F = 2.2 \cdot 10^{19} - 4 \cdot 10^{19}$ eV$^{-1} \cdot$ cm^{-3}) and energy spread of localized states ($\Delta E = 68$ meV), average time ($\tau = 5.7 \cdot 10^{-8}$ s), activation energy ($\Delta W = 0.62$ eV) and hop distance ($R = 56-77$ Å), as well as deep trap concentration ($N_t = 2.7 \cdot 10^{18}$ cm^{-3}), accountable for dc- and ac-conductivity in the $TlGaS_2:Nd^{3+}$ crystal.

Acknowledgments

The work has been partially funded by from the Science Development Foundation with the President of the Republic of Azerbaijan (EIF) (grant No. EIF-BGM-3-BRFTF-2+/2017-15/05/1-M-13) and the Russian Foundation for Basic Research (RFBR) (project No. Az_a2018).

Conflict of interest

The authors declare that they have no conflict of interest.

References

[1] S.N. Mustafaeva, V.A. Ramazanzade, M.M. Asadov. Mater. Chem. Phys. **40**, 142 (1995). https://doi:10.1016/0254-0584(94)01463-q

[2] S.N. Mustafaeva, M.M. Asadov, S.B. Kyazimov, N.Z. Gasanov. Inorgan. Mater. **48**, 1110 (2012). DOI: 10.1134/s0020168512090117

[3] S.N. Mustafaeva, M.M. Asadov, E.M. Kerimova, N.Z. Gasanov. Inorgan. Mater. **49**, 1175 (2013). https://doi:10.1134/s0020168513120121

[4] V.G. Gurtovoy, A.U. Sheleg, V.A. Chumak, S.N. Mustafaeva, E.M. Kerimova. Vestn. Grodennskogo gos. un-ta im. Ya. Kupaly. Ser. 2. Matematika. Fizika. Informatika, vychislitelnaya tekhnika i upravleniye **186**, 83 (2015) (in Russian).

[5] V.G. Gurtovoy, A.U. Sheleg, S.N. Mustafayeva, E.M. Kerimova. Izv. NAN Belarusi. Ser. fiz.-mat. nauk **2**, 98 (2015) (in Russian).

[6] S.N. Mustafaeva, K.M. Guseinova, M.M. Asadov. Phys. Solid State **62**, 1150 (2020). https://doi:10.1134/S1063783420070197

[7] R.E. Nikolaev, A.M. Chernovol, A.R. Tsygankova. Inorgan. Mater. **51**, 88 (2015). https://doi:10.1134/S0020168515020132

[8] E.F. Westrum, R.G. Burriel, B. John, P.E. Palmer, B.J. Beaudry, W.A. Plautz. J. Chem. Physics **91**, 4838 (1989). https://doi:10.1063/1.456722

[9] H. Yuan, J. Zhang, R. Yu, Q. Su. J. Rare Earths **27**, 308 (2009). https://doi:10.1016/s1002-0721(08)60239-2

[10] C.M. Forster, W.B. White. Mater. Res. Bull. **41**, 448 (2006). https://doi:10.1016/j.materresbull.2005.07.035

[11] S. Cwik, S.M.J. Beer, M. Schmidt, N.C. Gerhardt, T. Arcos, D. Rogalla, J. Weßing, I. Giner, M. Hofmann, G. Grundmeier, A.D. Wieck, A. Devi. Dalton Trans. **48**, 2926–2938 (2019). https://doi:10.1039/c8dt04317e

[12] D. Sofich, S.G. Dorzhieva, O.D. Chimitova, B.G. Bazarov, Yu.L. Tushinova, Zh.G. Bazarova, R.Yu. Shendrik. Phys. Solid State **61**, 844 (2019). https://doi:10.1134/S1063783419050342

[13] S.N. Mustafaeva, S.M. Asadov, E.M. Kerimova. Neorgan. materialy **54**, 662 (2018) (in Russian). https://doi:10.1134/s0020168518070099 [S.N. Mustafaevaa, S.M. Asadov, E.M. Kerimova. Inorg. Mater. **54**, *7*, 627 (2018)]. https://doi:10.1134/S0020168518070099

[14] H. Yuan, M. Ohta, S. Hirai, T. Nishimura, K. Shimakage. J. Rare Earths **22**, 759 (2004). https://doi.org/10.1016/S1002-0721(08)60239-2

[15] M. Ohta, S. Hirai, Z. Ma, T. Nishimura, Y. Uemura, K. Shimakage. J. Alloys Compd. **408**–**412**, 551 (2006). https://doi:10.1016/j.jallcom.2004.12.071

[16] M. Ohta, H. Yuan, S. Hirai, Y. Uemura, K. Shimakage. J. Alloys Compd. **74**, 112 (2004). https://doi:10.1016/j.jallcom.2003.11.081

[17] S.M. Asadov, S.N. Mustafaeva, V.F. Lukichev. Russ. Microelectron. **48**, 263 (2020). https://doi.org/10.1134/S1063739720040022

[18] M.M. Asadov, S.N. Mustafaeva, S.S. Guseinova, V.F. Lukichev, D.B. Tagiev. Phys. Solid State **63**, 797 (2021). https://doi.org/10.1134/S1063783421050036

[19] J.P. Perdew, K. Burke, M. Ernzerhof. Phys. Rev. Lett. **77**, 3865 (1996). https://doi.org/10.1103/physrevlett.77.3865

[20] J. Heyd, G.E. Scuseria, M. Ernzerhof. J. Chem. Phys. **118**, 8207 (2003). https://doi.org/10.1063/1.1564060

[21] J. Hubbard. Proc. Roy. Soc. London A **276**, 238 (1963). https://doi.org/10.1098/rspa.1963.0204

[22] S.M. Asadov, S.N. Mustafaeva. Phys. Solid State **60**, 499 (2018). DOI: 10.1134/S1063783418030034

[23] G.E. Delgado, A.J. Mora, F.V. Pérez, J. González. Physica B: Condens. Matter **391**, 385 (2007). https://doi:10.1016/j.physb.2006.10.030

[24] N. Sato, M. Odori, M. Skrobian, M. Saito, T. Fujino, N. Masuko. Shigen-to-Sozai **110**, 869 (1994). https://doi.org/10.2473/shigentosozai.110.869

[25] N.F. Mott, E.A. Davis. Electronic Processes in Non-Crystalline Materials. OUP Oxford, 2012. 590 p. ISBN: 9780199645336

[26] B.I. Shklovskii, A.L. Efros. Electronic Properties of Doped Semiconductors. Springer, Berlin, Heidelberg (1984). 393 p. ISBN: 978-3-662-02403-4

[27] M. Pollak. Phil. Mag. **23**, 519 (1971). https://doi.org/10.1080/14786437108216402

[28] V.V. Pasynkov, V.S. Sorokin. Materialy elektronnoy tekhniki. Vyssh. shk., M. (1986). 368 p. (in Russian).